THE ASTROPHYSICAL JOURNAL, 250:186–199, 1981 November 1

ABUNDANCES OF ARGON, SULFUR, AND NEON IN SIX GALACTIC H II REGIONS FROM INFRARED FORBIDDEN LINES

T. HERTER,[1,2] H. L. HELFER, AND J. L. PIPHER[2]
University of Rochester
W. J. FORREST, J. MCCARTHY, AND J. R. HOUCK
Cornell University
S. P. WILLNER, R. C. PUETTER, AND R. J. RUDY
Center for Astrophysics and Space Sciences, University of California at San Diego
AND
B. T. SOIFER
California Institute of Technology
Received 1980 December 12; accepted 1981 May 7

ABSTRACT

Airborne measurements of the [Ar II] (6.99 μm) and [S III] (18.71 μm) lines for six compact H II regions are presented, as well as ground-based 2–4 μm and 8–13 μm spectroscopy if not already published. From these data and radio data, we deduce lower limits to the elemental abundances of Ar, Ne, and S. G29.9 − 0.0 at 5 kpc from the galactic center is overabundant in all these elements. The other five regions (at distances 6–13 kpc from the center) mainly appear to be consistent with standard abundances, with the exception of G75.84 + 0.4 at 10 kpc from the galactic center, which is overabundant in S. However, our preliminary results on G12.8 − 0.2 at 6 kpc from the galactic center suggest a possible underabundance. We feel that a large statistical sample of H II regions is required in order to determine if there is a radial gradient in the heavy element abundances in our Galaxy.

Subject headings: infrared: spectra — nebulae: abundances — nebulae: H II regions

I. INTRODUCTION

We report here ground-based and airborne spectroscopic observations from 2 to 4 μm, 4 to 8 μm, 8 to 13 μm, and 16 to 30 μm for the compact H II regions G29.9–0.0, G45.1 + 0.1, G75.84 + 0.4, G12.8 − 0.2 (W33), NGC 7538 IRS2, and W3 IRS1. When available, the ground-based 2–4 μm and 8–13 μm data were gathered from the literature, and the new data were acquired at the Kitt Peak National Observatory (KPNO) and the Mt. Lemmon Observatory. The airborne 4–8 μm and 16–30 μm data were obtained on the Kuiper Airborne Observatory (KAO). Line fluxes at 6.99 μm [Ar II], 8.99 μm [Ar III], 10.51 μm [S IV], 12.81 μm [Ne II], and 18.71 μm [S III] are reported for these six H II regions, and estimates of the ionic abundances relative to hydrogen are deduced by using radio continuum data to obtain the ionized hydrogen column density.

The infrared fine-structure lines are well suited for abundance analysis for two reasons. First, the infrared line strengths are comparatively insensitive to the electron temperature, so that the temperature correction techniques employed at optical wavelengths (e.g., Peimbert 1975) are not required. Second, infrared lines provide a probe to much larger distances from the Sun than possible with optical lines, although substantial extinction corrections must still be made. The H II regions listed above range in galactocentric radii from 5 kpc to 13 kpc. A goal of this long range program is to search for possible abundance gradients in the Galaxy.

In spite of these advantages, it has become increasingly evident that a moderately complete data set is required to derive elemental abundances from observations of the infrared fine-structure lines. Relatively simple models of the ionization structure employing densities and excitation parameters consistent with radio observations are at variance with ground-based observations of the [Ar III], [S IV], and [Ne II] line strengths (Zeilik 1977; Balick and Sneden 1976; Lacasse *et al.* 1980). In addition, previous airborne observations of the [S III] and [Ar II] lines (McCarthy, Forrest, and Houck 1979; Puetter *et al.* 1979) indicate that S III is more abundant than S IV, and Ar II is also a primary ionization state, contrary to expectations if the ionizing source is a single hot star. Hence, observation of more than one ionization state of sulfur and argon is required for abundance analysis, and this allows an indirect probe of the UV radiation field in the nebula.

[1] Fannie and John Hertz Foundation Fellow.
[2] Visiting Astronomer at Kitt Peak National Observatory, Tucson, Arizona, operated by the Association of Universities for Research in Astronomy, Inc., under contract with the National Science Foundation.

II. OBSERVATIONS

The data described here were obtained with a variety of infrared systems. The 2–4 μm and 8–13 μm data were primarily obtained either at KPNO or the Mt. Lemmon Observatory using circular variable filter wheel (CVF) spectrometers with resolutions $\Delta\lambda/\lambda \sim 0.015$–$0.02$. These data are mainly published results, and new results are noted in Table 1. Sampling densities are typically one to two data points per resolution element.

The 4–8 μm data reported here consist of observations in the [Ar II] line and adjacent continuum using the University of California at San Diego (UCSD) filter wheel spectrometer (Russell, Soifer, and Willner 1977*a*; Puetter *et al.* 1979) on

TABLE 1

LINE FLUXES

Object	Line	$\bar{\tau}_\lambda$[a]	Measured Line Flux[b] (10^{-18} W cm^{-2})	Aperture (arc sec)	Reference	Line Flux Corrected for Extinction (10^{-18} W cm^{-2})
G29.9−0.0	Ar III	1.75 ± 0.25	13.0 ± 2.8	22	1	74.8 ± 24.7
	S IV	1.85 ± 0.26	<6.6[c]	22	1	<42
	Ne II	0.79 ± 0.11	113.8 ± 14.9	22	1	250 ± 42.9
	S III	1.31 ± 0.18	41.5 ± 4.3	30	2	153.8 ± 32.0
	Ar II	0.66 ± 0.09	22 ± 4	27	2	42.6 ± 8.6
	Brα	...	>3.8	17	2	...
	Brγ	...	0.76 ± 0.10	17	2	...
G75.84+0.4	Ar III[d]	1.68 ± 0.08	1.53 ± 0.37	11	3	8.2 ± 2.0
	S IV[d]	1.77 ± 0.08	1.98 ± 0.22	11	3	11.6 ± 1.0
	Ne II[d]	0.76 ± 0.04	4.58 ± 0.47	11	3	9.8 ± 1.0
	S III	1.26 ± 0.06	52.2 ± 3.6	30	2	184 ± 11
	Ar II	0.63 ± 0.03	6.0 ± 2.5	27	2	11.3 ± 2.5
	Brα	...	1.56 ± 0.20	11	3	...
	Brγ	...	0.25 ± 0.03	11	3	...
G12.8−0.2)	Ar III	3.44	0.69 ± 0.72	11	4	21.5 ± 22.4
	S IV[e]	3.64	0.97 ± 0.33	15	2	36.9 ± 12.3
	Ne II[e]	1.55	20.3 ± 1.7	15	2	95.6 ± 8.0
	S III	2.58	8.84 ± 2.02	30	2	116.7 ± 26.4
	Ar II	1.29	6.8 ± 1.7	27	2	24.7 ± 6.2
	Brα	...	1.1 ± 0.2	11	5	...
	Brγ	...	0.054 ± 0.016	11	5	...
G45.1+0.1	Ar III	1.62 ± 0.27	9.15 ± 2.02	...	6	46.2 ± 16.2
	S IV	1.71 ± 0.29	9.69 ± 2.13	...	6	53.6 ± 19.5
	Ne II	0.73 ± 0.12	30.8 ± 2.9	...	6	63.9 ± 9.8
	S III	1.21 ± 0.20	15.8 ± 1.9	30	2	53.0 ± 12.4
	Ar II	0.61 ± 0.10	5.2 ± 2.6	27	2	9.6 ± 4.9
	Brα	...	5.3 ± 0.4	11	4	...
	Brγ	...	0.89 ± 0.03	11	4	...
NGC 7538 (IRS2) ..	Ar III	0.96 ± 0.22	1.5 ± 1.3	11	4	3.9 ± 3.5
	S IV	1.01 ± 0.23	<3.9	11	4	<10.8
	Ne II	0.43 ± 0.10	20 ± 2.0	11	4	30.8 ± 4.4
	S III	0.72 ± 0.17	5.8 ± 2.8	30	2	11.8 ± 6.0
	Ar II	0.36 ± 0.08	13 ± 13	27	2	18.6 ± 18.6
	Brα	...	<0.3	17	7	...
	Brγ	...	0.18 ± 0.05	17	7	...
W3 (IRS1)	Ar III	1.50 ± 0.23	5.7 ± 0.98	11	8	25.8 ± 7.4
	S IV	1.59 ± 0.25	5.7 ± 1.06	11	8	28.2 ± 8.8
	Ne II	0.68 ± 0.10	9.79 ± 2.02	11	8	19.3 ± 4.4
	S III	1.13 ± 0.17	95.8 ± 7.5	30	2	297 ± 56
	Ar II	0.56 ± 0.09	4.7 ± 1.9	27	2	8.2 ± 3.4
	Brα	...	9.8 ± 0.2	22	9	...
	Brγ	...	1.6 ± 0.2	22	9	...

[a] From Tables 2 and 3.

[b] For details of line fits see text; two continuum points and a single point at 6.97 μm were used for the Ar II line fits.

[c] Upper limits are 3 σ.

[d] A partial spectrum obtained recently by blind offsetting to the nominal radio peak, rather than "peaking up", yields Ar III and S IV line fluxes similar to those listed here, while the Ne II flux is about a factor of 2 larger. The shape of the spectrum also indicates $\tau_{9.7} > 3$, larger than the value adopted in the present analysis.

[e] Measurements from 15″ partial spectrum as noted in text.

REFERENCES.—(1) Soifer and Pipher 1975. (2) Observations presented in this paper. (3) Pipher, Soifer, and Krassner 1979. (4) Provided by F. C. Gillett. (5) Pipher and Willner 1981. (6) Weighted average of Hefele and Schulte in den Bäumen 1978 and Pipher, Soifer, and Krassner 1979; only the latter data are plotted in Fig. 3. (7) Soifer, Russell, and Merrill 1976. (8) Lacasse *et al.* 1980. (9) Krassner and Pipher 1980.

flights of the KAO in 1979 June. For these observations a 27″ focal plane aperture was employed, and the chopped beam spacing and orientation were chosen to avoid beam cancellation.

The 16–30 μm data consist of complete spectra obtained with the Cornell University cooled grating spectrometer (McCarthy, Forrest, and Houck 1979) on flights of the KAO in 1979 June. A focal plane aperture of 30″ and choice of beam throw similar to that used with the UCSD instrument were employed. The spectral resolution over the [S III] line is 0.2 μm, sampled at a density of approximately three points per resolution element.

The observed line fluxes (uncorrected for extinction) are listed in Table 1 along with the beam sizes and references for the observations. The line fluxes for all but [Ar II] have been derived from a detailed fit to each line of the form $F_\lambda = a + b\lambda + c \exp - [(\lambda - \lambda_c)/\sigma_\lambda]^2$; that is, a linear continuum plus line emission at $\lambda = \lambda_c$, and $\sigma_\lambda \sim 0.6\Delta\lambda_{\rm FWHM}$, where $\Delta\lambda_{\rm FWHM}$ was determined from laboratory measurements. We vary a, b, and c to minimize

$$\chi^2 = \Sigma\left(\frac{F_{\rm obs} - F_{\rm model}}{\rm error}\right)^2 .$$

In one case (G29.9 − 0.0), a linear continuum was inadequate, and a quadratic continuum was assumed. For [Ar II] only one point in the line and one on either side in the adjacent continuum were used to estimate the line flux. The complete spectra from 2 to 30 μm are presented in Figures 1–3. In plotting these spectra, when different beam sizes were employed in different wavelength regions, we have *not* attempted to correct for beam size effects, since the ionization structure of the region prohibits simple scaling of the line intensities.

The spectra of Figures 1–3 show a number of emission and absorption features superposed upon the strong continuum primarily generated by dust. Atomic emission lines addressed in this paper include Brγ (2.17 μm), Brα (4.05 μm), and the fine-structure lines of [Ar II], [Ar III], [S IV], [Ne II], and [S III]. In addition, recombination lines of He I (2.06 μm) and Pfγ (3.76 μm) are visible in the spectrum of W3 IRS1. A number of continuum features are also visible. The familiar 9.7 μm silicate feature is clearly in absorption in G29.9 − 0.0, G12.8 − 0.2, and G45.1 + 0.1, and in emission in NGC 7538 IRS2. The associated 18 μm silicate absorption feature is not immediately evident to the eye, but it can be understood in terms of compensating emission and absorption features at 18 μm. Unidentified continuum emission features at 3.3, 6.2, 7.7, 8.6, and 11.3 μm have been detected in a variety of astronomical sources (Russell, Soifer, and Willner 1977*b*) and are seen in several of these spectra. Finally the 2–4 μm spectrum of NGC 7538 which includes both IRS1 and IRS2 shows a strong continuum absorption feature at ~ 3 μm, which is attributed to grain mantle molecules undergoing O–H, N–H, and C–H stretching vibrations. On the basis of the 8–13 μm spectra, and the 2.2 and 3.5 μm photometry, most of the continuum flux and the absorption are probably due to IRS1.

III. DISCUSSION

a) The Extinction

In order to compute the line fluxes from the H II regions, the infrared spectra must be corrected for extinction, which can be substantial. Depending on the wavelength, there are several ways of computing the extinction. At 2.17 μm (Brγ) and 4.05 μm (Brα), hydrogen recombination lines are observed and can be compared with radio continuum measurements of free-free radiation, or the ratio of the Brα and Brγ lines can be employed to compute the extinction. At 8–13 μm, the broad absorption feature seen in spectra is assumed due to cool silicate material in the line of sight. By use of an assumed extinction law, extinction at wavelengths between 4 and 8 μm can be extrapolated from shorter and longer wavelengths. At wavelengths longer than 13 μm, we adopt the value of $\tau_{18}/\tau_{9.7}$ determined by Forrest, McCarthy, and Houck (1979) from circumstellar shell data. This ratio is consistent with the value derived from simple two-component dust models of H II regions (McCarthy, Forrest, and Houck 1980). The adopted extinction law is presented in Table 2 and discussed below.

The 8–13 μm data have been corrected for extinction due to cool silicate material external to the line-emitting region by two simplified models. One of these (model I) assumes that hot grains radiate as blackbodies, and the other (model II) assumes optically thin silicate emission (Gillett *et al.* 1975*a*; Soifer and Pipher 1975). These models were computed by minimizing

$$\chi^2 = \Sigma'\left(\frac{F_{\rm obs} - F_{\rm model}}{\rm error}\right)^2 .$$

Generally the model II better fit the H II region discussed here. Limitations of these models have been discussed by Kwan and Scoville (1976) and Willner (1977). Also Jones *et al.* (1980) have shown that the trough between the unidentified 11.3 and 8.7 μm emission features mimics the silicate absorption feature at 9.7 μm in NGC 7027, and they suggest that the presence of unidentified features in a compact H II region spectrum might lead to an overestimate of the silicate optical depth. In Table 3 we list the computed model II fit of $\tau_{9.7}$ for each H II region studied. The Trapezium spectral shape (Gillett *et al.* 1975*a*) is used to determine $\tau_\lambda/\tau_{9.7}$ from 8 to 13 μm.

The 4–8 μm data have been treated in several ways. First, at 8 μm, there is overlap with the 8–13 μm data, and the extinction at 8 μm can be obtained through fitting the silicate feature from 8–13 μm as described briefly above. Second, the line flux to the radio continuum flux $\mathcal{F}$(Brα)/S_ν(radio) can be used to deduce the extinction at 4.05 μm if the Brα line is

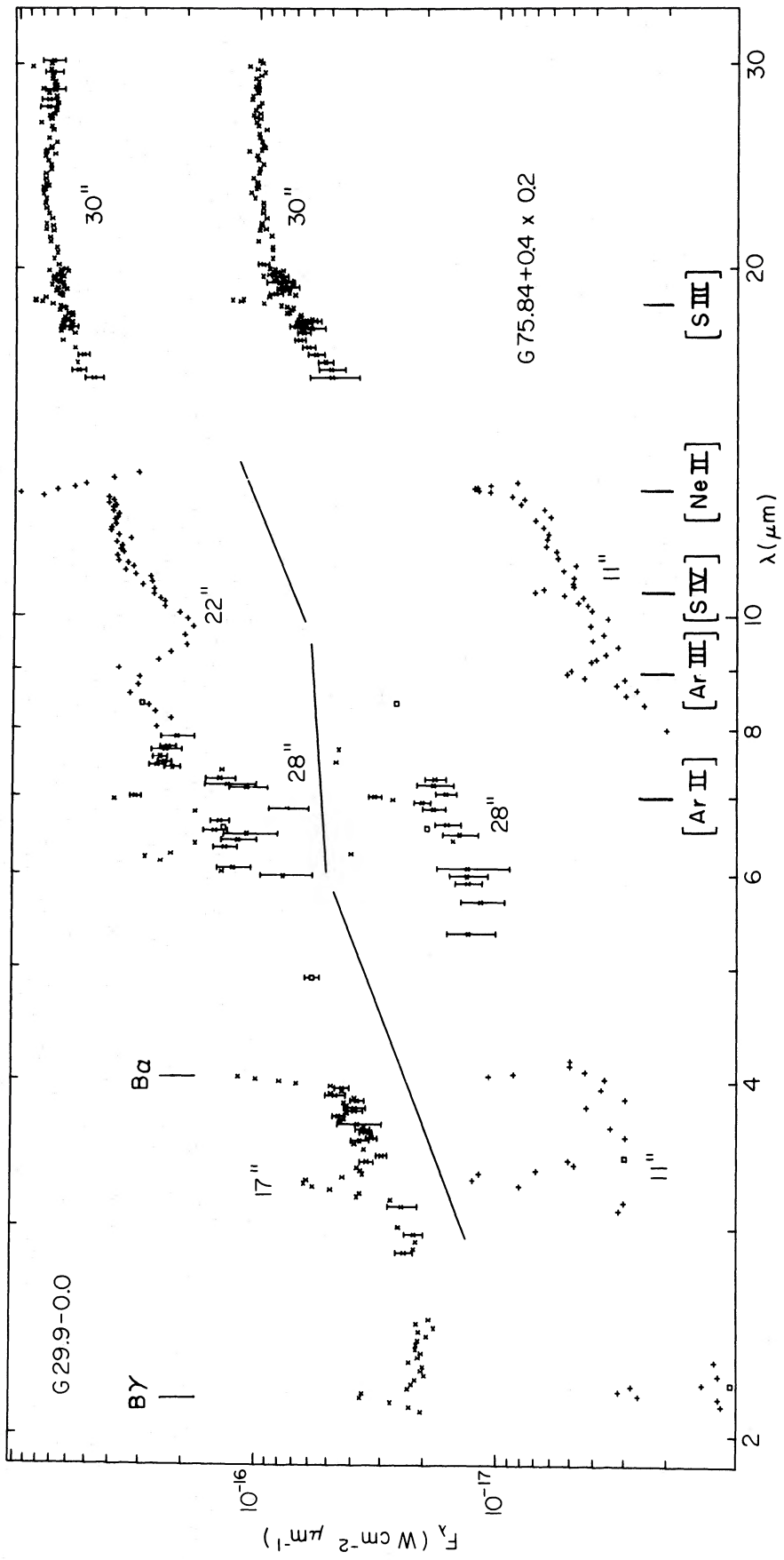

FIG. 1.—The 4–8 μm and the 16–30 μm data for G29.9 −0.0 and G75.84 +0.4, and the 2–4 μm data for G29.9 −0.0 were obtained as described in text. The 8–13 μm data for G29.9 −0.0 are from Soifer and Pipher 1975, and for G75.84 +0.4 from Pipher, Soifer, and Krassner 1979. The 2–4 μm data are from Pipher, Soifer, and Krassner 1979. Plots from the literature do not include error bars. Apertures for the observations plotted are marked on the figure.

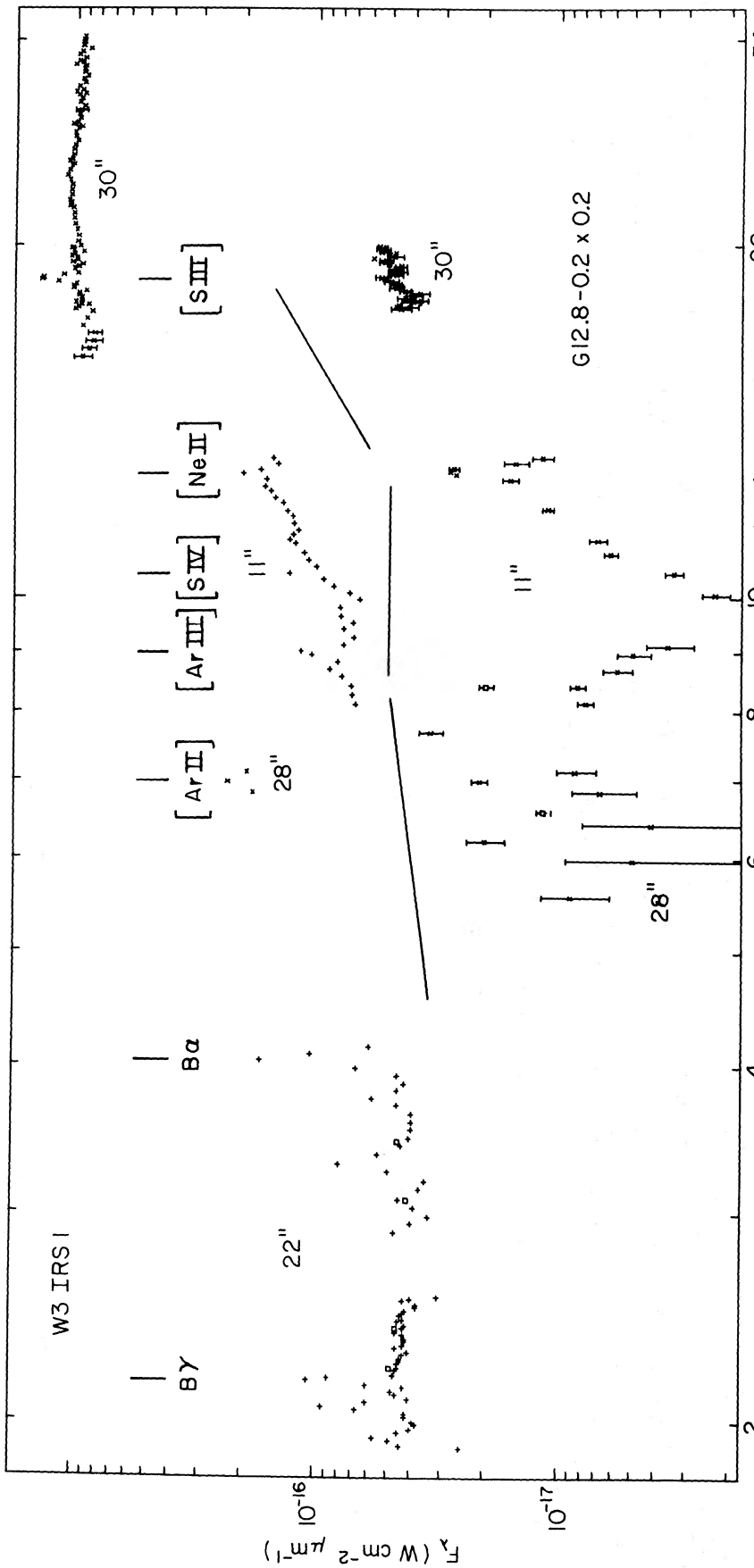

FIG. 2.—The 4–8 μm and 16–30 μm data for W3 IRS1 and G12.8 − 0.2 were obtained as described in text. The 8–13 μm data for W3 IRS1 are from Lacasse *et al.* 1980, and for G12.8 − 0.2 are provided by Gillett. The 2–4 μm data for W3 IRS1 are from Krassner and Pipher 1980. Plots from the literature do not include error bars. Apertures for the observations plotted are marked on the figure.

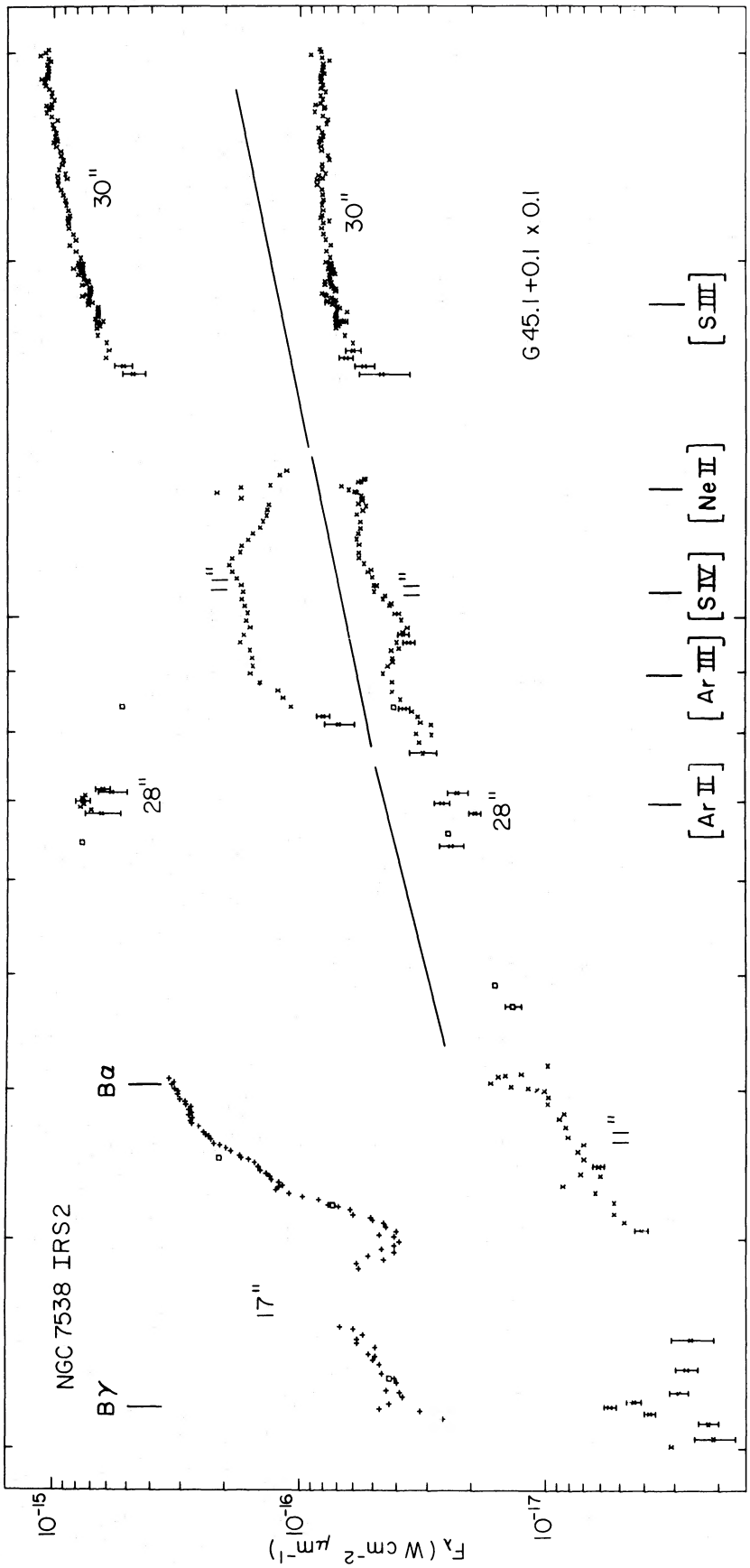

FIG. 3.—The 4–8 μm and 16–30 μm data for NGC 7538 IRS2, and G45.1+0.1 were obtained as described in text. The 8–13 μm data for NGC 7538 IRS2 and G45.1+0.1 are provided by Gillett and with better than 5% accuracy, so error bars are not plotted. The 2–4 μm data for NGC 7538 IRS2 are from Soifer, Russell, and Merrill 1976 and for G45.1+0.1 from Krassner and Pipher 1980. Plots from the literature do not include error bars. Apertures for the observations plotted are marked on the figure. Note that all the apertures except for the 8–13 μm data include IRS1 as well as IRS2 for NGC 7538, so that continuum levels disagree.

TABLE 2

ADOPTED EXTINCTION LAW

λ (μm)	Line	$\tau_\lambda/\tau_{9.7}$
1.25	...	2.21
1.65	...	1.31
2.17	Brγ	0.98
4.05	Brα	0.52
6.99	Ar II	0.30
8.99	Ar III	0.80
10.51	S IV	0.845
12.81	Ne II	0.36
18.71	S III	0.60

TABLE 3

COMPUTATION OF EXTINCTION[a]

Object	$\tau_{2.17}$[b]	$\tau_{4.05}$[c]	$\tau_{2.17}$[c]	$\tau_{9.7}$ (Model II)	$\tau_{1.25}$	$\tau_{1.65}$	$\bar{\tau}_{9.7}$[d]
G29.9−0.0	...	<0.94(<1.8)	1.5(1.5)	2.5	3.8(1.7)	2.3(1.8)	1.9 ± 0.4
G75.84+0.4	2.16(2.2)	...	...	2.0	...	...	2.1 ± 0.1
G45.1+0.1	1.60(1.6)	1.27(2.4)	1.99(2.0)	2.0	...	...	2.0 ± 0.3
NGC 7538 IRS2	...	...	1.15(1.2)	1.0	...	...	1.2 ± 0.3
W3 IRS1	1.8(1.9)	0.94(1.7)	1.7(1.8)	2.3	...	...	1.9 ± 0.3
G12.8−0.2	4.23(4.3)	...	...	4.3	...	...	4.3

[a] Quantities in parenthesis indicate $\tau_{9.7}$ determined from that value of τ_λ.
[b] From $\mathcal{F}$(Brγ)/$\mathcal{F}$(Brα).
[c] From $\mathcal{F}$(Brγ)/S_ν and $\mathcal{F}$(Brα)/S_ν.
[d] The errors are standard deviations.

detected. Alternately, one can use the Brγ line at 2.17 μm.[3] This technique has been used by a number of authors (e.g., Simon, Simon, and Joyce 1979; Soifer, Russell, and Merrill 1976) to determine the extinction. In some instances we have used the ratio of $\mathcal{F}$(Brα)/$\mathcal{F}$(Brγ) instead. This ratio is not very sensitive to the value of T_e assumed and does not necessitate estimating the radio flux in our beam. Both methods weight regions of lower optical depth if there is differential extinction across the beam. (The adopted Brα and Brγ fluxes are listed in Table 1.) Some assumed or measured value of the extinction law between 4 and 8 μm is then required to correct the data. The Van de Hulst number 15 reddening law approximates observed values from visual wavelengths out to 3–4 μm; beyond 4 μm the data are scarce and controversial. For example, Hackwell and Gehrz (1974) find a law consistent with $A_\lambda \propto \lambda^{-1}$ out to 10 μm (within the error bars), and the ratio $R = A_v/E_{B-V} = 3.4$ (rather than 3.1 for Van de Hulst number 15). The data of Gillett *et al.* (1975*b*) on VI Cygni Star 12 are also consistent with $A_\lambda \propto 1/\lambda$ from 4 to 8 μm; hence, we use this law to extrapolate to 6.99 μm from either 4 or 8 μm. From 16 to 30 μm the only available data are from the paper by Forrest, McCarthy, and Houck (1979) on circumstellar shells. They conclude that $\tau_{18.7} \sim 0.6\tau_{9.7}$. Because extinction corrections are so important in our abundance calculations, we have computed $\tau_{9.7}$ from $\tau_{2.17}$ and/or $\tau_{4.05}$ when the data were available using $\tau_\lambda/\tau_{9.7}$ and have deduced a mean value of the optical depth at 9.7 μm, $\bar{\tau}_{9.7}$, for use in further calculations, which is tabulated in Table 3, along with the standard deviation. This value of $\bar{\tau}_{9.7}$ is then employed with the assumed extinction law $\tau_\lambda/\tau_{9.7}$ to calculate the extinction at the wavelengths of the forbidden lines of Ar III, Ar II, Ne II, S III, and S IV. Table 1 presents line fluxes corrected for the extinction by this method. The corrected fluxes are used later in the abundance analysis. All of the uncertainties quoted for the corrected line fluxes, and ultimately the abundances (see next section), include our estimated uncertainty in the adopted $\bar{\tau}_\lambda$. The remaining uncertainty is the assumption that the extinction law is the same from region to region.

b) Estimating Ionic Abundances

In order to convert corrected line strengths into abundances, we follow the techniques of Petrosian (1970) and compute

$$\left\langle \frac{N_x^i}{N_H} \right\rangle = \frac{\int N_x^i N_e dV}{\int N_e N_H dV} = \frac{\int (N_x^i/N_H) N_e N_H dV}{\int N_p N_e dV}, \quad (1)$$

which gives an average abundance of element x in the ith ionization state with respect to hydrogen, weighted by the electron density N_e. In this expression, N_x^i is the ionic number density, and N_H is the hydrogen number density. If N_e is

[3] The assumed values of $\mathcal{F}$(Brα)/S_ν(5 GHz) and $\mathcal{F}$(Brγ)/S_ν(5 GHz) are 3.2×10^{12} Hz and 1.1×10^{12} Hz respectively at an electron temperature of 7500 K and are approximately proportional to $(T_e)^{-0.85}$ and $(T_e)^{-0.75}$, respectively. These ratios are not sensitive to the electron density and were calculated for He/H = 0.15, with no He^{++}.

TABLE 4

ADOPTED COLLISION STRENGTHS (Ω)

Ion	Transition	Ω
Ne II	$^2P_{1/2}$–$^2P_{3/2}$	0.368
S III	$^3P_1$–$^3P_0$	1.17
	$^3P_2$–$^3P_0$	0.56
	$^1D_2$–$^3P_0$	0.55
	$^1S_0$–$^3P_0$	0.11
	$^3P_2$–$^3P_1$	2.72
	$^1D_2$–$^3P_1$	1.64
	$^1S_0$–$^3P_1$	0.33
	$^1D_2$–$^3P_2$	2.74
	$^1S_0$–$^3P_2$	0.54
	$^1S_0$–$^1D_2$	1.29
S IV	$^2P_{3/2}$–$^2P_{1/2}$	1.66
Ar II	$^2P_{1/2}$–$^2P_{3/2}$	0.74
Ar III	$^3P_1$–$^3P_2$	2.21
	$^3P_0$–$^3P_2$	0.51
	$^1D_2$–$^3P_2$	2.55
	$^1S_0$–$^3P_2$	0.37
	$^3P_0$–$^3P_1$	1.12
	$^1D_2$–$^3P_1$	1.53
	$^1S_0$–$^3P_1$	0.22
	$^1D_2$–$^3P_0$	0.51
	$^1S_0$–$^3P_0$	0.074
	$^1S_0$–$^1D_2$	0.83

NOTE.—The preceding list was complied by W. J. Forrest. The Ne II collision strength was computed from calculations of Seaton 1975, while all other collision strengths are calculated from the data of Krueger and Czyzak 1970.

constant, and the integrals are evaluated over the entire H II region, then the above ratio is the actual ionic abundance. For density fluctuations, the abundance is weighted towards regions of higher radio flux. Using the expression for the radio flux S_ν, given by Osterbrock (1974) in the optically thin limit, and the line flux

$$F_l = \frac{1}{D^2}\int \left(\frac{j}{N_x{}^i N_e}\right)\frac{N_x{}^i}{N_H} N_e N_H dV\,, \tag{2}$$

where j is the emissivity in ergs cm^{-3} s^{-1} sr^{-1}, we obtain (assuming $N_e/N_H = 1.15$)

$$\left\langle\frac{N_x{}^i}{N_H}\right\rangle = 3.53\times 10^{-6}\left(\frac{F_l}{10^{-18} W\ \mathrm{cm}^{-2}}\right)\left(\frac{\nu}{5\ \mathrm{GHz}}\right)^{-0.1}\left(\frac{T_e}{7500\ \mathrm{K}}\right)^{-0.35}\left(\frac{S_\nu}{\mathrm{Jy}}\right)^{-1}\left(\frac{j/N_x{}^i N_e}{10^{-22}\ \mathrm{ergs\ cm^3\ s^{-1}\ sr^{-1}}}\right)^{-1}. \tag{3}$$

We assume an average value of $(j/N_x{}^i N_e)$ over the H II region ionization zone. The quantity $j/N_x{}^i N_e$ is obtained by solving the population balance equations (Osterbrock 1974) at the N_e and T_e of interest (obtained from radio continuum data), using the wavelengths and transition probabilities given by Osterbrock (1974). We use the collision strengths listed in Table 4 since the values tabulated by Osterbrock (1974) are in error for ions with $Z > 1$, and $T_e = 7500$ K (Forrest 1980). When employing equation (3) to compute ionic abundances, we use the line flux F_l corrected for extinction. Although use of $F_l/F_{\text{Brackett line}}$ would require a smaller differential extinction correction than F_l/S_ν, we wish to avoid the resulting dependence on electron temperature, which itself is abundance dependent.

In most cases cited here, the beam sizes for the Ar III, S IV, and Ne II measurements are *smaller* than the diameters of the H II regions. Because the ions being measured are not evenly distributed over the nebula, the computed ionic abundance from a small beam measurement (e.g., from only part of the H II region) does not necessarily reflect the *ionic* abundance for the entire H II region.

To illustrate how beam size effects for different ions of the same element are treated when combining ionic abundances, we imagine a situation in which only two ionization states [(1), (2)] of element x dominate the H II region. Then

$$\left\langle\frac{N_x}{N_H}\right\rangle = \frac{\int (N_x{}^{(1)}/N_H) N_e N_H dV + \int (N_x{}^{(2)}/N_H) N_e N_H dV}{\int N_e N_p dV}\,, \tag{4}$$

where the integrals are over any common volume (even if not the volume of the H II region). However, if common volumes are not sampled, we underestimate $\langle N_x/N_H\rangle$. For example, consider measurements of S III and S IV in an H II region with 30″ and 11″ apertures, respectively. These measurements can be combined to yield a lower limit to the

TABLE 5

$\langle N_x^i/N_H\rangle_{corrected}/N_x/N_{H\ standard}$[a]

Source	$\tau_{9.7}$[b]	Ar III	S IV	Ne II	S III	Ar II	Distance from Galactic Center (kpc)
G29.9−0.0	1.9 ± 0.4	1.9 ± 0.7	<0.2	1.8 ± 0.3	1.8 ± 0.7	3.1 ± 0.7	5
G12.8−0.2	4.3	0.46 ± 0.48	0.12 ± 0.04	0.30 ± 0.03	0.34 ± 0.08	0.32 ± 0.08	6
G45.1+0.1	2.0 ± 0.3	0.81 ± 0.28	0.22 ± 0.08	0.27 ± 0.04	0.53 ± 0.12	0.38 ± 0.20	7.5
G75.84+0.4	2.1 ± 0.1	0.63 ± 0.15	0.20 ± 0.02	0.18 ± 0.02	2.2 ± 0.1	0.72 ± 0.16	10
W3 (IRS1)	1.9 ± 0.3	1.7 ± 0.5	0.44 ± 0.14	0.32 ± 0.07	1.1 ± 0.2	0.15 ± 0.06	12
NGC 7538 (IRS2)	1.2 ± 0.3	0.29 ± 0.26	0.03 ± 0.06	0.55 ± 0.08	0.49 ± 0.25	3.2 ± 3.2	13

NOTE.—Adopted standard abundances relative to hydrogen: $N_{argon}/N_H = 4.7 \times 10^{-6}$; $N_{sulfur}/N_H = 1.6 \times 10^{-5}$; and $N_{neon}/N_H = 1.5 \times 10^{-4}$; from Cameron 1973 and Kaler 1978.

[a] Deduced as discussed in text: always referenced to beam sizes for the measurement. Errors include uncertainties from infrared line flux determinations and standard deviation of errors in τ (Table 3) but do *not* include those resulting from uncertainties in estimating radio flux for that volume.

[b] From Table 3.

elemental sulfur abundance by assuming that a minimum estimate of the amount of S IV that would be observed in a 30″ beam is the amount observed in the 11″ beam. If S and L represent the smaller and larger beams respectively, then

$$\left\langle \frac{N_x}{N_H} \right\rangle \geq \frac{\int_S (N_x^{(1)}/N_H) N_e N_H dV}{\int_L N_e N_H dV} + \frac{\int_L (N_x^{(2)}/N_H) N_e N_H dV}{\int_L N_e N_H dV} = \left\langle \frac{N_x^{(1)}}{N_H} \right\rangle_S \frac{V_S}{V_L} + \left\langle \frac{N_x^{(2)}}{N_H} \right\rangle_L . \quad (5)$$

V_S/V_L is the ratio of the radio fluxes in the small and large beams and the inequality is present because all of the S IV (ion number 1) may not be contained within the smaller aperture. If the S IV ion is distributed beyond 11″, the underestimate is substantial. However, if the S IV is completely contained within 11″, the equality holds, and we have a good estimate of the sulfur abundance. A further complication is the neglect of other ionization states, which also leads to an underestimate of the elemental abundance. However, without empirical knowledge of the ionization structure, these abundance estimates are the best possible. Correction factors designed to improve the abundance estimate by including a guess at the ionization structure are model dependent (see, e.g., Lacasse *et al.* 1980) and will not be employed here.[4] If clumping is present, $j/N_e N_x^i$ may decrease due to collisional de-excitation which also leads to an abundance underestimate.

Using the expression for $\langle N_x^i/N_H\rangle$, the line fluxes corrected for extinction from Table 1, and values of S_ν (justified below) for the same beam sizes as used in the IR measurements, we list the computed ionic abundances for the six H II regions studied in Table 5 relative to the standard elemental abundance. For comparison we adopt as our standard abundances (i.e., solar neighborhood) the values of Cameron (1973) for S/H, O/H and Kaler (1978) for Ar/O, Ne/O.

c) *Individual Sources*

In this section, we discuss computation of the ionic abundances for each of the individual sources and justify the choice of S_ν used in the computation; radio data for each source are given in Table 6. We emphasize at the outset that the choice of S_ν for extended sources is uncertain due to both the difficulties of obtaining integrated fluxes for our beams from radio maps with relatively poor resolution and the lack of knowledge concerning the exact infrared beam positions on the H II regions. We have no satisfactory method of deducing the amount of this uncertainty; hence, it is not included in our error estimates. However, this problem should be kept in mind when interpreting the final results. In what follows, we adopt a value of $T_e = 7500$ K for the electron temperature. Electron temperatures quoted (from radio recombination line studies) in the literature are quite discrepant (e.g., Lichton, Rodriquez, and Chaisson 1979; Churchwell *et al.* 1978) and have large uncertainties. The H II regions closer to the galactic center may have lower temperatures (due to presumed higher abundances); this point is currently under debate (Silvergate and Terzian 1979). Because this study is attempting to assess the existence of abundance gradients in the Galaxy, we do not a priori assume a temperature gradient.

i) *G29.9−0.0*

Spectrophotometric data from 8 to 13 μm have been previously obtained for G29.9−0.0 by Soifer and Pipher (1975). These investigators found a 12.6 μm half-power diameter of 13″ which agrees with that determined by Felli, Tofani, and D'Addario (1974) and Krassner *et al.* (1980) from radio continuum observations. Thus we can assume that both the airborne measurements of [Ar II] and [S III] line fluxes (27″, 30″ beams) and the ground-based measurements (22″ beam)

[4] As a guide to the reader, the Ar^+/Ar^{++} and/or S^{++}/S^{+++} ratios observed for G29.9−0.0, G12.8−0.2, G75.84+0.4, and NGC 7538 IRS2 suggest that the ionic abundance for Ne^+ should be roughly within a factor of 2 of the total Ne abundance.

TABLE 6

RADIO DATA

Source (1)	θ_s (arc sec) (2)	E (10^6 cm^{-6} pc) (3)	N_e (10^{+4} cm^{-3}) (4)	U (cm^{-2} pc) (5)	Flux (Jys) Total (6)	11″ (7)	27″ (8)	ν (GHz) (9)	References[d] (10)
G29.9−0.0	13[a]	7.7	0.4	75	2.9	~2.9	2.9	10.7	(1)
G75.84+0.4	22	6.8	0.34	66	3.7 ± 0.4	1.3	3.7	5	(2)
	11.7 × 6.9				2.54			2.7	(3)
G12.8−0.2	~35	34	0.8	100	25 ± 3	5.3	19.3	5	(4), (5)
G45.1+0.1	9.1	57	1.2	110	4.0 ± 0.3	~4.0	4.0 ± 0.3	5	(6)
NGC 7538 (IRS2)	10.9 × 7.8	14	1.1	31	1.4 ± 0.1	~1.4	1.4	5	(7)
	7.6[b]	20	1.3	36	1.3 ± 0.2	1.3	1.3	5	(8)
W3 (IRS1)	40 × 40[c]	...	0.6	92	33 ± 4	1.5	~12–14	5	(9), (10)

[a] Gaussian half-power width.

[b] Cylindrical geometry (diameter-length).

[c] Rough estimate from radio map.

[d] REFERENCES.—(1) 16″.1 × 250″ beam; Felli, Tofani, and D'Addario 1974. (2) Component A, 7″.2 × 9″.0 beam; Matthews *et al.* 1973. (3) Total flux, 9″.4 × 5″.5 beam; Turner *et al.* 1974. (4) G12.80−0.20, 5″.6 × 30″ beam; Goss, Matthews, and Winnberg 1978. (5) VLA measurements of T. Herter and J. Krassner 1980. (6) Component A, 7″ × 38″ beam; Matthews *et al.* 1977. (7) Component A, 2″.0 × 2″.3 beam; Martin 1973. (8) Component G2, 7″.5 × 8″.7 beam; Israel 1977. (9) W3A, 2″.0 × 2″.3 beam; Harris and Wynn-Williams 1976. (10) Wynn-Williams 1971.

of [Ar III], [S IV], and [Ne II] line fluxes were made with beams which encompassed the entire H II region. This allows direct computation of the ionic abundances. A 2–4 μm spectrum obtained at Mt. Lemmon on three nights from 1977–1979 is shown in Figure 1 along with other spectra noted above.

The radio flux density, S_ν, used in the abundance calculations is that of Felli, Tofani, and D'Addario (1974), who found a total flux of 2.9 Jy at 10.7 GHz. A recent VLA measurement of G29.9−0.0 by Herter and Krassner (1980) yielded 2.8 Jy at 5 GHz.

The extinction to G29.9−0.0 has been computed in a variety of ways. First, the model II fit to the 8–13 μm data of Soifer and Pipher (1975) yields $\tau_{9.7} = 2.5$. Because there is line emission from unidentified features at 3.3 μm, 6.2 μm, and 7.7 μm, one wonders whether a smaller value of $\tau_{9.7}$ might be appropriate. However, there is only marginal evidence for 8.7 and 11.3 μm features in the 8–13 μm spectrum of G29.9−0.0. Because we do not understand the nature of the emission features, and because the 11.3 μm feature is generally strong in H II regions where all features are present (Dwek *et al.* 1980), we consider the model II value of $\tau_{9.7}$ to provide an upper limit to the extinction. We can also compute the extinction from the radio and Brγ fluxes, assuming $T_e = 7500$ K and find that $\tau_{2.17} = 1.5$ which implies $\tau_{9.7} = 1.5$. Because this value is quite different from the model II upper limit, we examine other independent methods of computing the extinction. Photometry at J and H, with a 17″ beam, yields value of 3.5×10^{-18} W cm^{-2} μm and 8.3×10^{-18} W cm^{-2} μm, respectively. Using the expressions developed by Willner, Becklin, and Visvanathan (1972) relating the predicted flux density in these bands relative to radio flux density on the assumption that only recombination processes contribute to the infrared flux density, we compute lower limits to the opacity at J and H of $\tau_{1.25} \geq 3.8$ and $\tau_{1.65} \geq 2.3$, respectively. These in turn lead to $\tau_{9.7} \geq 1.7$, 1.8 respectively, where the equality applies if there is no additional source of infrared radiation such as dust emission. We have assumed dust emission to be negligible at J and H and have adopted the average of the four extinction values derived above. The main remaining discrepancy is that we can compute a lower limit to the Brα flux (incomplete wavelength coverage of data) which implies $\tau_{9.7} < 1.8$. This is close to the adopted value of $\bar{\tau}_{9.7} = 1.9 \pm 0.4$, and either a lower electron temperature or a different extinction curve could resolve the remaining discrepancy. Such changes would act in a direction to *increase* the derived abundances.

We now compute the ionic abundances $\langle N_x/N_H \rangle$, using the corrected line fluxes F_l (assuming the average extinction correction $\bar{\tau}_{9.7}$) and the value of S_ν adopted. In Table 4, the ionic abundances are expressed as ratios with respect to the standard elemental abundances. Since the measurement beams encompass the H II region, the *sum* of the Ar II and Ar III abundance ratios represent a lower limit to the measured argon abundance ratio in G29.9−0.0, namely 5.0 ± 1.4 times standard argon abundance. Ar IV is also expected to be present in G29.9−0.0, although the nondetection of S IV suggests this may be a small constituent. We note that even if $\tau_{6.99\,\mu m} = 0$, Ar II alone is 1.6 times standard argon abundance, and thus argon is clearly overabundant in this source. The total sulfur abundance $\approx$ the S III abundance, and is 1.8 ± 0.7 times standard. Finally, the Ne II abundance is 1.8 ± 0.3 times the standard *elemental* neon abundance, indicating that neon is also overabundant. Furthermore, much of the neon is expected to be in the form of Ne III, based on the excitation parameter (Table 6). We note that if there is clumping, all of these abundance ratios would be even larger.

ii) *G75.84+0.4*

Spectrophotometric measurements of this source have been obtained by Pipher, Soifer, and Krassner (1979) in the spectral ranges from 2 to 4 μm and 8 to 13 μm (see Table 1, note e). A map at 12.6 μm by these authors and radio continuum mapping by Matthews *et al.* (1973) at 5 GHz (7″.2 × 9″ beam size) and Turner *et al.* (1974) at 2.7 GHz

(9″.4 × 5″.5 beam size) confirm the multiple structure of this source and indicate a general coincidence between the infrared and radio emission. Both radio measurements indicate two main components of comparable total flux and size. According to Matthews *et al.* (1973), component A is 19″ × 12″ with a total flux of 3.7 ± 0.4 Jy, while component B, which lies ~ 20″ to the east of A, is 20″ × 18″ and has a total flux of 2.7 ± 0.3 Jy. Turner *et al.* (1974) find a total flux of 1.6 Jy for component A and a total flux for all components added together of 2.5 Jy and note that G75.84+0.4 is probably optically thick at 2.7 GHz. Line flux measurements were taken with beams centered on component A; hence, this component will be the dominant contributor to the radio flux for the beam sizes of interest here (≤ 30″). We assume that for [Ar II] and [S III] line flux measurements the beam encompassed the entire H II region associated with component A. For computation of the [Ar III], [S IV], and [Ne II] abundances we estimate from the parameters for the H II region given by Matthews *et al.* (1973) that ~ 1.3 Jy at 5 GHz would be contained in a radio beam centered on component A with a beam size comparable to the infrared measurements (11″). (See, however, discussion by Turner *et al.* (1974) who find the physical parameters derived by Matthews *et al.* (1973) to be uncertain, because the complex may have multiple components. Hence the adopted values of S_ν in our beam size may be in error by as much as a factor of 2.)

According to Pipher, Soifer, and Krassner (1979) the value of $\tau_{9.7}$ is 0.5 or 2.1 depending whether a model I and model II fit is chosen (see § III*a*). Typically, the model II fit is the "best fit." But since neither χ^2 model fit was unambiguously better, we consider other extinction estimates. Because we are uncertain about the radio flux in our beam, we use the ratio of the Brγ and Brα line fluxes, coupled with the assumed extinction law, to deduce $\tau_{2.17} = 2.2$, which would imply $\tau_{9.7} = 2.2$. The 2–4 μm spectrum may have been obtained at a somewhat different spatial position, and variable extinction across the nebula is possible; hence, there may be some uncertainty in comparing these estimates of $\tau_{9.7}$. Despite the excellent agreement of the model II value with that determined from the Brackett lines, we adopt $\bar{\tau}_{9.7} = 2.15 \pm 0.3$. Here the error is not the formal standard deviation but a *typical* uncertainty in $\bar{\tau}_{9.7}$. Ionic abundances relative to the standards are listed in Table 4 for this mean value of $\tau_{9.7}$. Combining ionic abundances according to the prescription outlined in § III*b*, we find the following *lower* limits to the elemental abundances for argon and sulphur (relative to standard abundance), of 0.94 ± 0.21 and 2.3 ± 0.1 respectively. We can conclude that the *lower* limit to the abundance for Ar is consistent with the adopted standard abundance, within the errors, and S is a factor of 2 overabundant. Since other stages of ionization have not been observed (notably Ar IV and Ne III) and since not *all* of the H II region was sampled for *all* ions measured (see § III*b*), the resultant Ne and Ar abundances may even exceed standard values.

iii) *G45.1+0.1*

Spectrophotometric observations of G45.1+0.1 have been obtained by Krassner and Pipher (1980) and by F. C. Gillett from 2 to 4 μm with an 11″ beam and from 8 to 13 μm by Hefele and Schulte in den Bäumen (1978) and a 22″ beam. New observations from 8 to 13 μm are presented here (Fig. 3) with a 7″.5 beam (observations with an 11″ beam are identical in spectral shape and flux density). A radio continuum map of G45.1+0.1 at 5 GHz by Matthews *et al.* (1977) with a 7″ × 38″ beam size reveals two dominant components separated by ~ 50″. Component A is found to be ~6″.5 in size with a total flux of 4.0 ± 0.3 Jy,[5] whereas component B is 25″ in size with a total flux of 2.1 ± 0.3 Jy. All infrared line flux measurements were taken centered on component A; thus, due to the small source size, we expect *all* infrared beams to include all of component A, but none of B. The multiplicity of beam sizes for 8–13 μm measurements, which show no appreciable differences in forbidden line flux, also support this contention.

The ionic abundances are computed using a flux of 6.0 Jy at 5 GHz (see note 5) for component A and the corrected line fluxes for G45.1+0.1. An average (weighted by errors determined by the χ^2 line fits) of the line fluxes of Hefele and Schulte in den Bäumen (1978) and the present data has been adopted. Although the present data (11″ beam) show no apparent detection of [S IV] and [Ar III], Hefele and Schulte in den Bäumen (1978) detected these lines in a 22″ beam. The mean extinction correction ($\bar{\tau}_{9.7} = 2.0 \pm 0.3$) is listed in Table 3: it was deduced from the ratio of the Brγ and Brα line fluxes to the radio flux, the model II fit to the 8–13 μm measurements presented here, $\tau_{9.7} = 2.0$, and the assumed $\tau_\lambda/\tau_{9.7}$ extinction law. The corrected ionic abundances relative to hydrogen are listed in Table 5. Since all infrared beams are assumed to encompass the entire H II region, these ionic abundances can be combined to yield the elemental abundance (see § III*b*). This gives elemental abundance ratios for argon and sulphur (relative to standard) of 1.2 ± 0.5 and 0.75 ± 0.2, respectively. We conclude that the abundances for Ar, S, and Ne in G45.1+0.1 are consistent with the adopted standard abundances. If Ar IV and Ne III are present in any quantity, as is expected on the basis of the high excitation parameter (Table 6) and/or if there is clumping, the actual elemental abundances may very well exceed standard abundances.

NGC7538 IRS2

Southwest of the optical H II region NGC 7538 = S158 is a compact radio source which high resolution continuum measurements resolve into three distinct components. Martin (1973) has mapped this source at 5 GHz with 2″ resolution and finds component A (which is 8″.9 × 8″.0) with a total flux of 1.4 ± 0.1 Jy dominates components B and C which have total fluxes of only 0.12 ± 0.02 and 0.02 ± 0.01 Jy respectively. Israel (1977) finds similar results with lower resolution

[5] Matthews *et al.* (1977) find $\tau_{5\ \mathrm{GHz}} \approx 0.87$, thus equation (3), which assumes that S_ν is optically thin, is not directly applicable. Since the radio flux in the optically thin limit $= S_0\tau$, we can deduce an "equivalent" S_ν in this case, by multiplying the measured 4 Jy by $\tau/(1 - e^{-\tau})$. The "equivalent" S_ν is 6 Jy for use in equation (3).

($\sim 7''$) 5 GHz measurements. Wynn-Williams, Becklin, and Neugebauer (1974) have mapped this region at 20 μm with a 5″ beam and find infrared sources coincident with each of the radio sources found by Martin. Willner (1976) has obtained spectra from 8 to 13 μm of all three components with a 7.″5 beam and finds IRS2 to be the only source in the complex showing evidence of infrared forbidden line emission. A new 8–13 μm spectrum of IRS2 (provided by F. C. Gillett) was obtained with an 11″ beam. All of the other measurements were obtained with an observing aperture sufficiently large to encompass both IRS1 and IRS2. Thus there is a large discrepancy among the continuum levels plotted in Figure 3.

The line fluxes for IRS2 are listed in Table 1. [Ne II] is the only line unambiguously detected; formal fitting procedures give upper limits to the strengths of other lines. An extinction correction of $\tau_{9.7} = 1.0$ was determined from a model II fit to our 8–13 μm spectrum. Soifer, Russell, and Merrill (1976) observed the Brγ flux and using the appropriate value of $\mathcal{F}_{2.17}/S_{5\ \mathrm{GHz}}$ we find $\tau_{2.17} = 1.2$. From the adopted extinction law (Table 2), we deduce $\bar{\tau}_{9.7} = 1.2 \pm 0.3$. After correcting the [Ne II] line flux for extinction, we compute the Ne II abundance relative to standard for NGC 7538 IRS2, namely 0.55 ± 0.08. Because other stages of ionization may be present for neon (e.g., Ne III), we can only conclude that the measured ionic abundance of Ne II is consistent with the adopted standard abundance. For other ions (with the marginal exception of S III below), the signal-to-noise ratio is sufficiently poor to prohibit any conclusions.

The nearby optical H II region NGC 7538 has been observed for [S III] flux using the Lear Jet telescope with a 2.′7 beam (Forrest, Briotta, and Gull 1979). The beam was centered on the optical nebulosity and a flux of $19 \pm 3 \times 10^{-17}$ W cm^{-2} was observed in the 18.7 μm line. Using the 15 GHz radio data of Schraml and Mezger (1969), we estimate a radio flux of approximately 11.9 Jy from this region. As this region is optically visible, the extinction at 18.7 μm should be quite small. Then the above fluxes imply a S III abundance (relative to standard elemental sulfur abundance) of 0.82; our determination of the relative S III abundance from IRS2, where an extinction correction *was* employed, is 0.49 ± 0.25 (see Table 5). For comparison, Talent and Dufour (1979) derive a [S III] abundance of 0.46 standard from optical observations in two small regions and also derive a S II abundance of only 0.07 standard. As some of the sulfur may be in the form of S IV in this region, we conclude the [S III] measurements in NGC 7538 are compatible with the standard S abundance.

v) *W3 IRS1*

Spectrophotometric observations of W3 IRS1 have been obtained by Willner (1977) from 8 to 13 μm with an 11″ beam and by Krassner and Pipher (1980) from 2 to 4 μm and 8 to 13 μm with 22″ and 11″ observing apertures, respectively. The [Ar II] and [S III] data reported here were obtained with 27″ and 30″ apertures, respectively. A radio continuum map at 5 GHz with 2″ resolution by Harris and Wynn-Williams (1976) reveals a shell structure in the emitting gas approximately 40″ in diameter roughly centered in IRS2, the dominant exciting star (Harris and Wynn-Williams 1976). Due to the extended nature of this source, *none* of the infrared apertures include all of IRS1. The 2–4 μm and 8–13 μm spectra of Krassner and Pipher (1980), adopted here, and the [Ar II] measurement of this paper were acquired with the beams approximately centered on IRS2; we estimate from the radio map of Harris and Wynn-Williams (1976) that 5 GHz radio fluxes of 0, 1.5, and 13 Jy respectively would be contained in 22″, 11″, and 27″ apertures. The peak [S III] line flux was found to occur at the 5 GHz ridge to the northwest of IRS2. We estimate $\sim$ 13 Jy at 5 GHz will be contained in this observing aperture.

The measured line fluxes for W3 IRS1 are presented in Table 1. A model II fit to the 8–13 μm spectrum of Krassner and Pipher (1980) yields an extinction correction of $\tau_{9.7} = 2.3$. The ratios of the Brγ and Brα line fluxes to the radio flux in the same beam size imply $\tau_{2.17} = 1.7$ and $\tau_{4.05} = 0.9$. The ratio of the Brackett fluxes leads to $\tau_{2.17} = 1.8$. Because there is differential extinction across W3, these values all underestimate the optical depth. Nonetheless, we use these and the adopted extinction law, $\tau_\lambda/\tau_{9.7}$, to deduce $\bar{\tau}_{9.7} = 1.9 \pm 0.3$. Using the correct line fluxes (Table 1) and the appropriate value of S_ν, we derive the corrected ionic abundances relative to the adopted standard elemental abundances; these values are listed in Table 5.

If the ionic abundances are combined according to the prescription given in § III*b*, we find that the lower limit for sulphur relative to standard abundance is 1.2 ± 0.2. The observed ionic abundance of [Ar II] in a 28″ beam shows that this ion is neligible compared to [Ar III]. Thus the argon abundance is $\geq 1.7 \pm 0.5$ standard, suggesting the argon may be overabundant. We conclude that the abundances in W3 IRS1 of S and Ne are consistent with the adopted standard abundances, noting that models of W3 IRS1 suggest that the argon measurement is indeed a lower limit (Herter *et al.* 1981). A large aperture (2.′7) measurement by McCarthy (1980) yields S III abundance of 0.22 standard sulfur abundance (uncorrected for extinction). After correcting for extinction, this is in reasonable agreement with the value found here.

vi) *G12.8 − 0.2*

We present a new 8–13 μm spectrum (with an 11″ beam) of the strong thermal radio source G12.8 − 0.2 in the W33 complex as well as a 4–8 μm and 16–30 μm spectrum in Figure 2. A partial 8–13 μm spectrum using a 15″ beam was also obtained; the spectrum is not plotted in Figure 2, but the [Ne II] and [S IV] measurements are reported in Table 1. Goss, Matthews, and Winnberg (1978) find that this source dominates the complex with a radio flux at 5 GHz of 25 Jy and a radio size of $\sim 14'' \times 27''$. The other weaker compact sources in the complex ($\sim$ 12′ in diameter) contribute less than 2 Jy radio flux, although diffuse flux of $\sim$ 30 Jy spread over the 12′ diameter is indicated. Unfortunately, the highest resolution radio map available had a resolution of $5.6'' \times 30''$.[6]

[6] Our VLA data (resolution $\sim 2''$) on G12.8 − 0.2 are not yet complete. Preliminary analysis suggests that the source is larger than 30″ arc in diameter, and that 15%, 21%, 33%, and 76% of the total flux is contained in beams of 9″, 11″, 15″, and 30″ respectively.

The measured line fluxes are given in Table 1. A 2–4.3 μm spectrum of G12.8 − 0.2 has been obtained by Pipher and Willner (1981), and they estimate $\tau_{2.7} = 4.2$ from the ratio of $\mathcal{F}(\mathrm{Br}\alpha)/\mathcal{F}(\mathrm{Br}\gamma)$. From a model II fit to the 8–13 μm spectrum we find $\tau_{9.7} = 4.3$, in excellent agreement with the Brackett line estimate. A mean value of $\bar{\tau}_{9.7} = 4.3 \pm 0.1$ is assumed to correct the line fluxes. Using the adopted radio fluxes, and the corrected line fluxes, we deduce the corrected ionic abundances relative to elemental standard abundances (Table 5). Combining these according to the prescription in § III*b*, we find that the elemental abundances are 0.3 ± 0.1 times standard for Ar II, 0.4 ± 0.1 times standard for sulfur and 0.3 ± 0.03 times standard for neon. Because we have no information on other ionization states or clumping, we quote these abundances as lower limits. However, as noted below, a rather enigmatic situation exists for this source.

Though the above calculations indicate a possible underabundance of S III in G12.8 − 0.2, measurements of the same area with a 2'.7 beam gave a much larger [S III] flux than was found with the 28″ beam reported here. McCarthy (1980) reports $13 \pm 2 \times 10^{-17}$ W cm^{-2} for the [S III] 18.7 μm flux. This is about 16 times larger than the 28″ measurements. However, radio observations of this region indicate that most of the radio flux in a 2'.7 beam (Schraml and Mezger 1969; Altenhoff *et al.* 1978) which we estimate at about 25 Jy at 10 GHz, originates from the ~ 20″ diameter compact H II region (Felli, Tofani, and D'Addario 1974; Goss, Matthews, and Winnberg 1978). Since the radio emission should be a good tracer for the ionized gas in this region, it is not clear where the large S III flux observed in the 2'.7 beam is coming from. This property is similar to that found for W51, where the S III fluxes from the compact components IRS1 and IRS2 (Forrest 1980) provide only a small fraction of the flux seen in a 2'.7 beam (McCarthy, Forrest, and Houck 1979), even though the radio maps indicate that they dominate the thermal emission from that region.

The possibility that the small aperture observations somehow missed the compact H II region has been considered but does not seem likely. The position in the sky which was observed was determined by first offsetting from a nearby guide star to the nominal position of the H II region (Goss, Matthews, and Winnberg 1978) and then peaking up in the continuum around 19 μm. The final position gave a continuum 20 μm flux of about 2.8×10^{-16} W cm^{-2} μm^{-1} which, considering the beam sizes, is consistent with the flux of 2×10^{-16} W cm^{-2} μm^{-1} found by Dyck and Simon (1977) for their brightest component in this region (IRS3). In the process of peaking up, data on the strength of the 18.71 μm line in the immediate vicinity of the compact H II region were gathered. Though the peak up signal-to-noise ratio was not large ($S/N \sim 2/1$), within ± 15″ of the final peak the line flux was not significantly larger than at the final position. We conclude that we were pointed at the compact H II region.

The question of what is responsible for the relatively large [S III] line flux observed in the larger beam is an intriguing one. Because of the difficulty of separating a low surface brightness radio component from the very bright compact component with the data currently available, it is possible that the region viewed in the large beam had some thermal radio emission in addition to the 25 Jy from the compact component. The amount could not be large compared to the emission from the compact H II region. If we estimate an upper limit to its radio emission as $\lesssim 10$ Jy, then we estimate a S III abundance relative to standard sulfur abundance of $\geq 0.6 \times [\exp(\tau_{18.7})]$, where $\tau_{18.7}$ is the extinction to the region. *Thus even with no extinction assumed, the abundance of* S III *in the extended component appears to be at least a factor of 2 higher than in the compact* H II *region and is comparable to the standard abundance.* The source of this disparity is not understood at present. Some possible explanations are: (1) severe clumping in the compact H II region suppressing the S III flux; (2) a much larger optical depth to the compact H II region than has been assumed here—if the extinction is patchy across our beam size, we seriously underestimate $\tau_{9.7}$ by all the methods used; (3) an actual difference in the gaseous sulfur abundances between the compact H II region and the diffuse H II region. There is some controversy on the relative distances to the different components and we may be sampling two separated regions (Goss, Matthews, and Winnberg 1978). The [S IV] and Brackett measurements rule out substantially higher or lower excitation. We plan spatial observations of the complex in the Brα and [Ne II] lines and abjacent continua to attempt to resolve the disparity.

IV. CONCLUSIONS

We have gathered infrared line fluxes for [Ar II] (6.99 μm), [Ar III] (8.99 μm), [Ne II] (12.81 μm), [S III] (18.71 μm), and [S IV] (10.51 μm) in six compact H II regions well distributed in distance from the galactic center. Extinction to these regions was estimated by a variety of methods in order to arrive at a realistic value of the correction factor to apply to these measured line fluxes. The Ne, Ar, and S abundance for these regions are calculated by combining these data with radio data on the same objects; quoted errors in the calculated abundances include uncertainties in estimating the extinction. The two H II regions sampled close to the galactic center (G29.9 − 0.0 and G12.8 − 0.2) give quite different results. G29.9 − 0.0 appears to be overabundant in Ne, Ar, and S, while G12.8 − 0.2 appears to be roughly standard or underabundant in these elements. We believe that errors in the extinction have been carefully taken into consideration, and that this is not the cause of the abundance difference. However, it is possible that the radio fluxes used in these calculations do not exactly correspond to the radio flux contained in the infrared beam size. We are attempting to overcome this possible source of error through an extensive series of measurements on the VLA. Other regions with possible overabundance include G75.84 + 0.4 (in S) and W3 (in Ar), both at ≥ 10 kpc from the galactic center. Our limited data suggests region to region abundance variations. Abundance gradients determined optically (Peimbert, Torres-Peimbert, and Rayo 1978 and references therein) often show scatter of the same order of magnitude as the derived abundance gradients. Because of the small number of regions sampled and the uncertainties in interpreting the infrared line data (such as importance of clumping, neglect of other stages of ionization, and nature of the extinction law), we do

not propose to attempt an estimate of the alleged gradient. However, it is important to obtain more measurements of the type outlined here in greater detail (e.g., better spatial coverage and similar beam sizes) so that *total* abundances can be reliably estimated. We require a sufficiently large sample of such observations to assess statistically the abundance pattern in our Galaxy. The present results seem to indicate that the abundances of Ar, S, and Ne vary substantially from H II region to H II region, whatever the underlying reason.

We wish to thank the support staff of the Kuiper Observatory for their excellent performance during flight operations. We thank Dr. F. C. Gillett for providing unpublished data, and for his helpful comments on the manuscript. All of the authors are supported by grants from NASA and the NSF.

REFERENCES

Altenhoff, W. J., Downes, D., Pauls, T., and Schraml. J. 1978, *Astr. Ap. Suppl.*, **35**, 23.
Balick, B., and Sneden, C. 1976, *Ap. J.*, **208**, 336.
Cameron, A. G. W. 1973, *Space Sci. Rev.*, **15**, 121.
Churchwell, E., Smith, L. F., Mathis, J., Mezger, P. G., and Huchtmeier, W. 1978, *Astr. Ap.*, **70**, 719.
Dwek, E., Sellgren, K., Soifer, B. T., and Werner, W. M. 1980, *Ap. J.*, **238**, 140.
Dyck, H. M., and Simon, T. 1977, *Ap. J.*, **211**, 421.
Felli, M., Tofani, G., and D'Addario, L. R. 1974, *Astr. Ap.*, **31**, 431.
Forrest, W. J. 1980, private communication.
Forrest, W. J., Briotta, D. A., and Gull, G. E. 1979, private communication.
Forrest, W. J., McCarthy, J. F., and Houck, J. R. 1979, *Ap. J.*, **233**, 611.
Gillett, F. C., Forrest, W. F., Merrill, K. M., Capps, R. W., and Soifer, B. T. 1975*a*, *Ap. J.*, **200**, 609.
Gillett, F. C., Jones, T. W., Merrill, K. M., and Stein, W. A. 1975*b*, *Astr. Ap.*, **45**, 77.
Goss, W. M., Matthews, H. E., and Winnberg, A. 1978, *Astr. Ap.*, **65**, 307.
Hackwell, J. A., and Gehrz, R. P. 1974, *Ap. J.*, **194**, 49.
Harris, S., and Wynn-Williams, C. G. 1976, *M.N.R.A.S.*, **174**, 649.
Hefele, H., and Schulte in den Bäumen, J. 1978, *Astr. Ap.*, **66**, 465.
Herter, T., and Krassner, J. 1980, private communication.
Herter, T., Pipher, J., Helfer, H. L., Willner, S. P., Puetter, R. C., and Rudy, R. 1981, *Ap. J.*, **244**, 511.
Israel, F. P. 1977, *Astr. Ap.*, **59**, 27.
Jones, B., *et al.* 1980, preprint.
Kaler, J. B. 1978, *Ap. J.*, **225**, 527.
Krassner, J., and Pipher, J. L. 1980, in preparation.
Krassner, J., Pipher, J. L., Savedoff, M. P., and Soifer, B. T. 1980, in preparation.
Krueger, T. K., and Czyak, F. J. 1970, *Proc. Roy. Soc. London, A*, **318**, 531.
Kwan, J., and Scoville, N. 1976, *Ap. J.*, **209**, 102.
Lacasse, M., Herter, T., Krassner, J., Helfer, H. L., and Pipher, J. L. 1980, *Astr. Ap.*, **86**, 231.
Lichton, S. M., Rodriguez, L. F., and Chaisson, E. J. 1979, *Ap. J.*, **229**, 524.
Martin, A. H. M. 1973, *M.N.R.A.S.*, **163**, 141.
Matthews, H. E., Goss, W. M., Winnberg, A., and Habing, H. J. 1973, *Astr. Ap.*, **29**, 309.
Matthews, H. E., Goss, W. M., Winnberg, A., and Habing, H. J. 1977, *Astr. Ap.*, **61**, 261.
McCarthy, J. F., Ph.D. thesis, Cornell University.
McCarthy, J. F., Forrest, W. J., and Houck, J. R. 1979, *Ap. J.*, **231**, 711.
Osterbrock, P. E. 1974, *Astrophysics and Gaseous Nebulae* (San Francisco: Freeman).
Peimbert, M. 1975, *Ann. Rev. Astr. Ap.*, **13**, 113.
Peimbert, M., Torres-Peimbert, S., and Rayo, J. F. 1978, *Ap. J.*, **220**, 516.
Petrosian, V. 1970, *Ap. J.*, **159**, 883.
Pipher, J. L., Soifer, B. T., and Krassner, J. 1979, *Astr. Ap.*, **74**, 302.
Pipher, J. L., and Willner, S. P. 1981, in preparation.
Puetter, R. C., Russell, R. W., Soifer, B. T., and Willner, S. P. 1979, *Ap. J.*, **228**, 118.
Russell, R. W., Soifer, B. T., and Willner, S. P. 1979*a*, *Ap. J.*, **213**, 66.
———. 1977*b*, *Ap. J* (*Letters*), **217**, L149.
Seaton, M. J. 1975, *M.N.R.A.S.*, **170**, 475.
Schraml, J., and Mezger, P. G. 1969, *Ap. J.*, **156**, 269.
Silvergate, P. R., and Terzian, Y. I. 1979, *Ap. J. Suppl.*, **39**, 157.
Simon, T., Simon, M., and Joyce, R. R. 1979, *Ap. J.*, **230**, 127.
Soifer, B. T., and Pipher, J. L. 1975, *Ap. J.*, **199**, 663.
Soifer, B. T., Russell, R. W., and Merrill, K. M. 1976, *Ap. J.*, **210**, 334.
Talent, D. L., and Dufour, R. J. 1979, *Ap. J.*, **233**, 888.
Turner, B. E., Balick, B., Cudaback, D. D., Heiles, C., and Boyle, R. J. 1974, *Ap. J.*, **194**, 279.
Willner, S. P. 1976, *Ap. J.*, **206**, 728.
———. 1977, *Ap. J.*, **214**, 706.
Willner, S. P., Becklin, E. E., and Visvanathan, N. 1972, *Ap. J.*, **175**, 699.
Wynn-Williams, C. G. 1971, *M.N.R.A.S.*, **151**, 397.
Wynn-Williams, C. G., Becklin, E. E., and Neugebauer, G. 1974, *Ap. J.*, **187**, 473.
Zeilik, M. 1977, *Ap. J.*, **218**, 118.

H. L. HELFER, W. J. FORREST, and J. L. PIPHER: Department of Physics and Astronomy, University of Rochester, Rochester, NY 14627

T. HERTER, J. R. HOUCK, and J. MCCARTHY: Astronomy Department, Cornell University, Space Sciences Building, Ithaca NY 14853

R. C. PUETTER, R. J. RUDY, and S. P. WILLNER: Center for Astrophysics and Space Sciences, University of California at San Diego, C-011, La Jolla, CA 92093

B. T. SOIFER: Division of Physics, California Institute of Technology, Downes Lab 320-47, Pasadena, CA 91125